INTERNATIONAL JOURNAL FOR NUMERICAL METHODS IN FLUIDS
Int. J. Numer. Meth. Fluids 2001; **35**: 519–531

Prediction of unobstructed flow for co-rotating multi-disk drive in an enclosure

E. Y. K. Ng[a,*] and Z. Y. Liu[b]

[a] *School of Mechanical and Production Engineering, Nanyang Technological University, Singapore*
[b] *Data Storage Institute, Engineering Drive, National University of Singapore, Singapore*

SUMMARY

The flow structure and isotherms of hard disk drives (HDD) are investigated using a finite element method (FEM). The governing equations are based on the three-dimensional axisymmetric Navier–Stokes partial differential equations (PDEs) with Galerkin FE formulation. Co-rotating models are selected that include the non-ventilated configuration within an enclosure. With various operating conditions for the disk system, the following important parameters are considered: disk number (n), rotational speed (Ro), and wall temperature. The flow structure changes rapidly when the rotational Reynolds number (Re_ϕ) is increased. The flow has a greater tendency to flow radially outwards and the swirling velocity tends to be more vertically orientated, especially for high Re_ϕ values. The isotherms only have small varying regions near the rotating axis, forming outward arcs near the wall and inward arcs near the end gap of the disk. Different from the case without the enclosure, the vorticities exist along the outer disk ends. Both the swirling velocity and isotherms indicate nearly symmetrical characteristics, as expected. A higher temperature gradient occurs near the right outer disk ends, which implies the characteristic of higher heat flux. A commercial computational fluid dynamic (CFD) code, CFX-5, was chosen to validate the results. Copyright © 2001 John Wiley & Sons, Ltd.

KEY WORDS: hard disk drives; isotherm and flow structures; finite element method; Navier–Stokes equations

1. INTRODUCTION

Rotating flow and its heat transfer have been a topic of concern for long time. As far back as in 1889, Brayan [1] wrote about the problem of rotating liquid. Batchelor [2] and Stewartson [3] presented different types of flow structure of rotating disks later. Theoretical and experimental researches were also developed by Owen and Rogers [4], Morse [5], Northrop *et al.* [6], and Tzeng *et al.* [7]. The computer industry's rapid development in the post-1970s years has brought the hard disk system into an intensive area of research, especially as the capacity

* Correspondence to: School of Mechanical and Production Engineering, Nanyang Technological University, 50, Nanyang Avenue, Singapore 639798, Singapore.

Received July 1999
Revised February 2000

demand and rotating speed have been becoming higher and faster. As a result, the flow structure and heat transfer problems between the disk space have received increased attention recently. Yang [8] and Soong [9], for example, have focussed on such co-axial disks related to them.

The rotation-induced buoyancy with the density variation has effects on the rotating thermal system. While the Coriolis effect produced due to the fixed reference frame with one disk can also affect the flow and heat transfer (both of which have been investigated by Soong [10], who used a pseudo-transient procedure based on the artificial pressure for pressure-linked equations (APPLE) algorithm by finite volume method (FVM)), only laminar flows were considered in it. It was shown that the Coriolis effect enhanced heat transfer performance, however, the centrifugal buoyancy might degrade it, although its influence was not very remarkable. It also concluded that the shroud clearance and the relative rotation rate of the disks markedly affected the flow structure.

As for the turbulent flows, Morse *et al.* [11] made an assessment for the laminar–turbulent transition in closed disk geometries and investigated the transport phenomena in non-isothermal flow between co-rotating disks [12], where the k–ε equations model was used. Although the k–ε model has been proved to be effective on many fields, it is criticized when involved in situations with curved or rotational flows. This problem was solved with the renormalization group (RNG) method by Yakhot and Orszag [13] in 1986 to analyze the turbulent flow by determining the constants analytically from assumptions about the shape of the energy spectrum. This RNG-based k–ε model was applied and later improved by Thangam and Speziale [14,15], with good results when compared with the predictions of the experimental data. Zhu [16] also used this method with an artificial compressibility algorithm to examined the benchmark problem of backward-facing step flow.

In the present work, the RNG-based k–ε turbulence model and artificial compressibility algorithm are used in the standard Galerkin finite element formulation. A new language called *Fasttalk*, which is supported by a finite element PDE calculator, *Fastflo*, is then implemented and the results are compared with other published data.

As a general PDE solver, *Fastflo*'s main advantage is its flexibility in specifying models and algorithms to solve them. An internal mesh generator is also built in supplying a range of isoparametric element types. The whole computation process can be controlled intelligently. It allows users to create or modify a finite element environment for individual needs. There is no need for time-consuming programming in languages; in *Fasttalk*, the problem description is concise, although the main detailed steps of the algorithm are still requirements.

2. PROBLEM AND GOVERNING EQUATIONS

As for the non-ventilated flow which is more similar to the real hard disk configuration without the entering fluid, these models are investigated and all disks have the same rotational speed, as shown in Figure 2. The basic assumptions involved are

1. disks are heated isothermally;
2. Boussinesq's approximation is invoked;

3. the flow is steady, turbulent, axisymmetric and of constant properties;
4. a linear density–temperature relationship is used to account for the centrifugal buoyancy; and
5. a gravity factor can be included in the pressure gradient but is ignored here for its weak effect as compared with other force terms.

For the standard incompressible RNG-based k–ε turbulence model, the axisymmetric governing cylindrical co-ordinate Navier–Stokes equations in (r, θ, z) can be written as

$$\frac{\partial u_i}{\partial x_i} = 0 \tag{1}$$

$$u_j \frac{\partial u_i}{\partial x_j} = -\frac{\partial p}{\partial x_i} + \frac{\partial}{\partial x_j}\left[v_t \left(\frac{\partial u_i}{\partial x_j} + \frac{\partial u_j}{\partial x_i} \right) \right] \tag{2}$$

$$u_j \frac{\partial T}{\partial x_j} = v_t \nabla^2 T \tag{3}$$

$$u_j \frac{\partial k}{\partial x_j} = \alpha v_t \nabla^2 k + v_t \frac{\partial u_i}{\partial x_j} \left(\frac{\partial u_i}{\partial x_j} + \frac{\partial u_j}{\partial x_i} \right) - \varepsilon \tag{4}$$

$$u_j \frac{\partial \varepsilon}{\partial x_j} = \alpha v_t \nabla^2 \varepsilon + C_1 v_t \frac{\varepsilon}{k} \frac{\partial u_i}{\partial x_j} \left(\frac{\partial u_i}{\partial x_j} + \frac{\partial u_j}{\partial x_i} \right) - C_2 \frac{\varepsilon^2}{k} - R \tag{5}$$

where

$$x_i \ \ (i = 1, 2, 3) = (r, \theta, z)$$

$$\nabla^2 = \frac{1}{r} \frac{\partial}{\partial r} \left(r \frac{\partial}{\partial r} \right) + \frac{\partial^2}{\partial z^2}$$

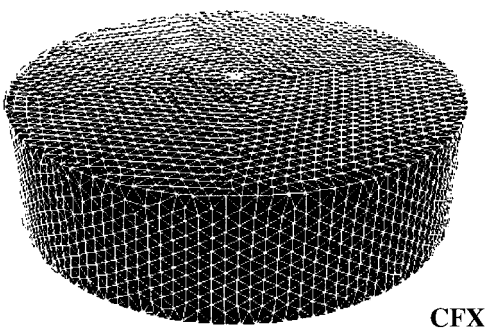

Figure 1. FVM three-dimensional surface mesh for four co-rotating disks within a cylindrical enclosure.

$$R = \frac{C_\mu \eta^3 (1 - \eta/\eta_0)}{1 + \beta \eta^3} \frac{\varepsilon^2}{k}, \quad \eta = \frac{Sk}{\varepsilon}, \quad S = 2S_{ij}S_{ij}$$

$$S_{ij} = \frac{1}{2}\left(\frac{\partial u_i}{\partial x_j} + \frac{\partial u_j}{\partial x_i}\right)^2$$

R is the rate of strain term.

The effective viscosity is

$$v_t = v + C_\mu \frac{k^2}{\varepsilon} \quad \text{or} \quad v_T = \frac{v}{P_r} + \frac{C_\mu}{\sigma_T}\frac{k^2}{\varepsilon}$$

where v is the molecule viscosity, k is the turbulence kinetic energy and ε is the turbulence dissipation rate. The constants used in the RNG model are $C_\mu = 0.0845$, $C_1 = 1.42$, $C_2 = 1.68$, $\alpha = 1.39$, $\beta = 0.012$, $\eta_0 = 4.38$, $\sigma_T = 1.0$.

3. NUMERICAL ALGORITHM

In this paper, the artificial compressibility method with the upwinding scheme is applied in a standard Galerkin finite element formulation.

3.1. Artificial compressibility method

For the steady incompressible laminar flows, the continuity and Navier–Stokes equations (1) and (2) have the form (after introducing the artificial compressibility items [17])

$$\nabla \cdot V + \frac{1}{\beta}\frac{\partial P}{\partial t} = 0 \tag{6}$$

$$\frac{\partial V}{\partial t} + (V \cdot \nabla)V + \nabla P = \frac{1}{Re}\Delta V \tag{7}$$

If you let $V^{n+1} = V^n + \mathrm{d}V^n$ and $P^{n+1} = P^n + \mathrm{d}P^n$, Equations (6) and (7) can be written as the numerical formulation

$$\beta\ \mathrm{d}t(\nabla \cdot \mathrm{d}V^n) + \mathrm{d}P^n + \beta\ \mathrm{d}t(\nabla \cdot V^n) = 0 \tag{8}$$

$$(V^n \cdot \nabla)\,\mathrm{d}V^n + (\mathrm{d}V^n \cdot \nabla)V^n + \nabla\,\mathrm{d}P^n - \frac{1}{Re}\Delta\,\mathrm{d}V^n + (V^n \cdot \nabla)V^n + \nabla P^n = \frac{1}{Re}\Delta V^n \tag{9}$$

where the symbol t is used to denote time and β is used to control the amount of compressibility. When using Equations (8) and (9) as the iterative process, it should be noted that for the first iteration, full values of all boundary conditions are applied to the equation system, and for iteration level $N > 1$, all the values of the boundary conditions should be set to zero.

3.2. Upwinding scheme and $k-\varepsilon$ turbulence model

When the artificial compressibility method is used in the $k-\varepsilon$ equations with the standard Galerkin finite element formulation, the temporal terms are used to stabilize the iterative process with respect to the pseudo-time of the artificial compressibility method. The iterative process in solving the governing equations involves

(i) Momentum equations (2) are solved to provide velocity components u_i $(i = 1, 2, 3)$

$$\sum_j u_j^n \frac{\partial u_i^{n+1}}{\partial x_j} - \sum_j \frac{\partial}{\partial x_j}\left[\nu_t \frac{\partial u_i^{n+1}}{\partial x_j}\right] - \frac{\partial}{\partial x_i}\left[(\mathrm{d}t\cdot\lambda + \nu_t)\frac{\partial u_j^{n+1}}{\partial x_j}\right] - \sum_j \sum_k \frac{\partial}{\partial x_j}\left[K_{jk}^n \frac{\partial u_i^{n+1}}{\partial x_k}\right] - \sum_j \frac{\partial \nu_t}{\partial x_j}\frac{\partial u_j^{n+1}}{\partial x_i} = -\frac{\partial P^n}{\partial x_i} + \frac{\partial u_j^n}{\partial x_j}\frac{\partial \nu_t}{\partial x_i} \tag{10}$$

Here, the artificial compressibility parameters are $\lambda = 5.0$, $\mathrm{d}t = 0.1$. At each iteration, the velocity component, u_i, is treated as the unknown variable. The artificial diffusion tensor is chosen as $K_{ij}^n = (\mathrm{d}t/2)u_i^n u_j^n$ during the initial iteration process and $K_{ij}^n = (\mathrm{d}t/2)\,\mathrm{d}u_i^n\,\mathrm{d}u_j^n$ when the solution is close to convergence.

The boundary conditions u_i $(i = 1, 2, 3)$ prescribed along the disks; $u_i = 0$ for solid wall boundaries.

(ii) From the velocities newly obtained using the iterative equation (10), the scalar continuity equation is then solved to give the pressure increment $\mathrm{d}P$

$$\mathrm{d}P^{n+1} - \frac{\mathrm{d}t^2\cdot\theta}{2}\Delta\,\mathrm{d}P^{n+1} = -\mathrm{d}t\cdot\lambda\sum_j \frac{\partial u_j^{n+1}}{\partial x_j} + \frac{\mathrm{d}t^2\cdot\lambda}{2}\Delta P + \frac{\mathrm{d}t^2\cdot\lambda}{2}\nabla\cdot[(V^{n+1}\cdot\nabla)V^{n+1}] - \mathrm{d}t^2\cdot\lambda\sum_i\sum_j \frac{\partial}{\partial x_i}\left[\frac{\partial \nu_t}{\partial x_j}\frac{\partial u_j^{n+1}}{\partial x_i}\right] - \mathrm{d}t^2\cdot\lambda\sum_i \frac{\partial}{\partial x_i}\left[\nu_t \frac{\partial}{\partial x_i}\sum_j \frac{\partial u_j^{n+1}}{\partial x_j}\right] \tag{11}$$

(iii) The k transport equation can then be solved in the following form:

$$\frac{\partial k^{n+1}}{\partial t} + \sum_j u_j^{n+1}\frac{\partial k^{n+1}}{\partial x_j} - \sum_j \frac{\partial}{\partial x_j}\left[\alpha\nu_t \frac{\partial k^{n+1}}{\partial x_j}\right] - \sum_i\sum_j \frac{\partial}{\partial x_i}\left[K_{ij}^{n+1}\frac{\partial k^{n+1}}{\partial x_i}\right] + \frac{\varepsilon^n}{k^n}k^{n+1} = \nu_t \sum_{ij}\frac{\partial u_i^{n+1}}{\partial x_j}\left(\frac{\partial u_i^{n+1}}{\partial x_j} + \frac{\partial u_j^{n+1}}{\partial x_i}\right) \tag{12}$$

At the solid wall, $\partial k/\partial n = 0$.

(iv) Finally, the ε transport equation is solved

$$\frac{\partial \varepsilon^{n+1}}{\partial t} + \sum_j u_j^{n+1} \frac{\partial \varepsilon^{n+1}}{\partial x_j} - \sum_j \frac{\partial}{\partial x_j}\left[\alpha v_t \frac{\partial \varepsilon^{n+1}}{\partial x_j}\right] - \sum_i \sum_j \frac{\partial}{\partial x_j}\left[K_{ij}^{n+1} \frac{\partial \varepsilon^{n+1}}{\partial x_i}\right] + C_2 \frac{\varepsilon^n}{k^{n+1}} \varepsilon^{n+1}$$
$$= C_1 v_t \sum_{ij} \frac{\varepsilon}{k} \frac{\partial u_i^{n+1}}{\partial x_j}\left(\frac{\partial u_k}{\partial x_j} + \frac{\partial u_j^{n+1}}{\partial x_i}\right) - R \tag{13}$$

The boundary conditions for ε equations are:

At solid wall $\varepsilon = C_\mu k^2 v_{\text{mol}}/y^+$, where $y^+ = 16$–30, v_{mol} is the molecule viscosity, $C_1 = 1.42$, $C_2 = 1.68$.

Both the k and ε equations have to be factorized for each iteration for non-linear characteristics.

This RNG-based k–ε model is used throughout the whole flow region as the same governing equations for k and ε are integrated to the solid boundary wall directly. In other words, flows with separation zones can be captured more accurately by not invoking the 'law of wall' [18].

In view of the axisymmetric problem, each variable does not change in the same circumferential co-ordinate θ. Thus, in each of the circular θ-directions, all the differentiation terms are zero. However, there is the variation in the r–z plane and distribution of velocity in the w-component is allowed. In other words, velocity w has a direction in the tangential direction, but its variation can only exist in the two-dimensional r–z plane.

The numerical computation was performed using an SGI workstation with various flow conditions. Several specific parameters are given, such as the convergence criterion, with $\varepsilon = 10^{-3}$ and the total iteration number $N\text{STEP} = 1400$ with averaged CPU time of 0.00275 s/point per time step.

4. RESULTS AND DISCUSSION

Some parameters are defined as follows: Re_ϕ (rotational Reynolds number) $= \Omega_1 R^2/v$; Gr (rotational Grashof number) $= \Omega_1 S^4 \beta (T_w - T_i)/v^2$; δ_i (for multi-disk system) $= (\Omega_i - \Omega_1)/\Omega_1$.

First, a two-disk system was investigated. As shown in Figure 3, the vorticities focus mainly along the zone of the outer disk end and the gap between the disks and the enclosure. They are also more obvious in the space of the central two disks. This phenomenon is also similar for the streamline in the three- (Figure 6) and four-disk systems (Figure 9), except in the four-disk system there are few vorticities within the disk space. Note that vorticity–contour or streamfunction plots are recommended as any difference/similarity can be clearly discerned.

The swirling velocities for the three systems (Figures 4, 7 and 10) are quite different. With the higher disk number, the velocity profile between the disks becomes more uniform, especially in the four-disk system (Figure 10) where the contours are almost perpendicular.

The isotherm profile changes when the rotational speed is increased. In Figure 5, the rotational Reynolds number is $Re_\phi = 0.55 \times 10^4$, the isotherms are almost horizontal with a lower gradient. When Re_ϕ is increased to 1×10^4, the gradients of the isotherm profile concentrate on the outer disk end, where arcs appear (Figure 8). This phenomenon is more prominent for the four-disk system as presented in Figure 11.

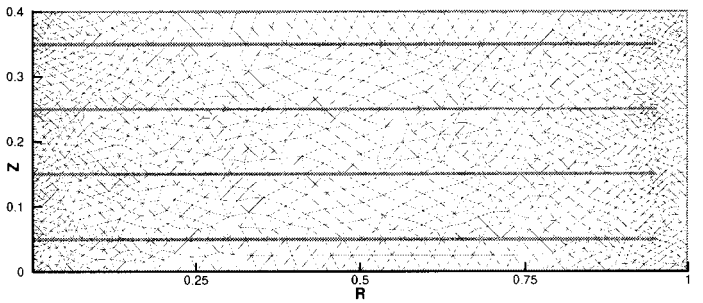

Figure 2. FE mesh for four co-rotating disks within a cylindrical enclosure.

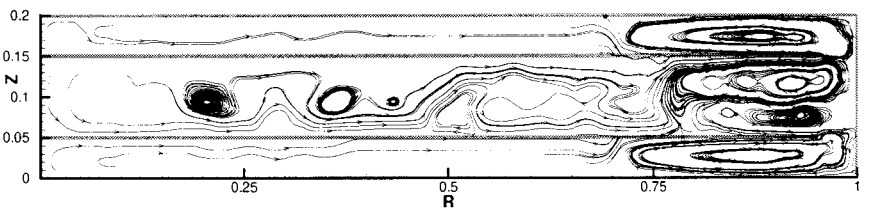

Figure 3. Streamline for a two-disk system with $Re_\phi = 0.55 \times 10^4$, $Gr = 0.03 \times 10^4$, $\delta_i = 0$ $(i = 2)$.

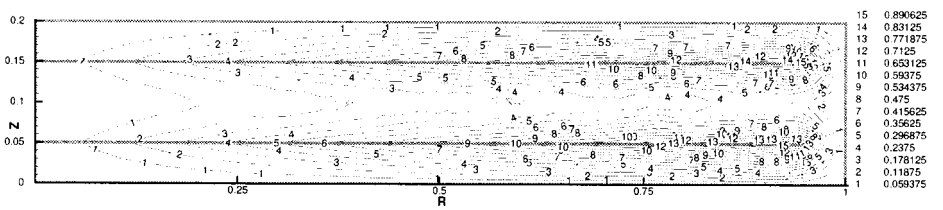

Figure 4. Swirling velocity for a two-disk system with $Re_\phi = 0.55 \times 10^4$, $Gr = 0.03 \times 10^4$, $\delta_i = 0$ $(i = 2)$.

5. VALIDATION USING A COMMERCIAL CODE

Since the prediction is so updated, not a lot of experimental data are available for comparison. The commercial software CFX-5 [19] was used to validate the results. CFX-5 is a popular FVM CFD code combining an advanced solver with powerful pre- and post-processing capabilities. Using the CFX-builder, the complex geometry can be created. After the boundary conditions have been defined, the unstructured surface and volume mesh can be generated accordingly, which depend on the mesher used. Before the modelling, the suitable parameters

should be selected: flow pattern, fluid properties, initial values, etc. After the computation, a CFX-visualize can be used to manipulate the different plots using the data computed by the CFX-solver.

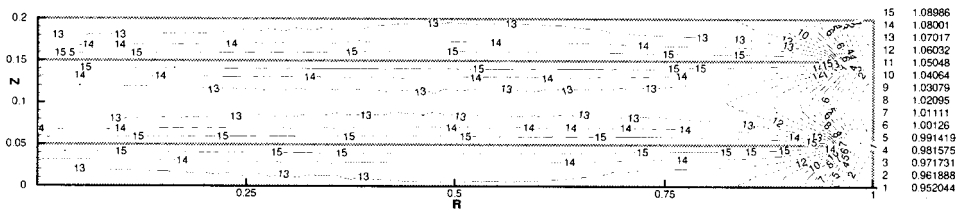

Figure 5. Isotherms for a two-disk system with $Re_\phi = 0.55 \times 10^4$, $Gr = 0.03 \times 10^4$, $\delta_i = 0$ $(i = 2)$.

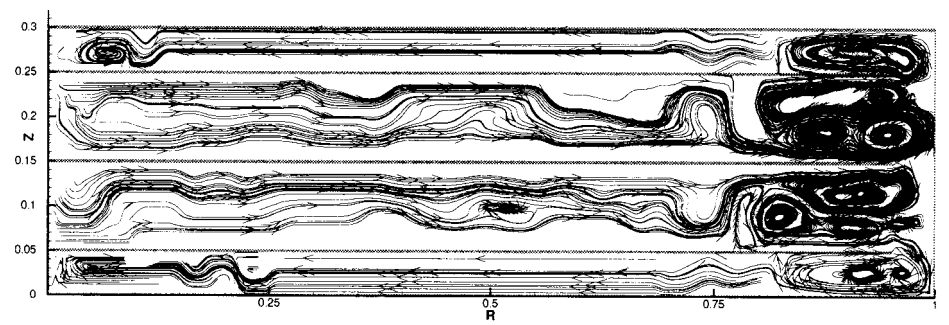

Figure 6. Streamline for a three-disk system with $Re_\phi = 1 \times 10^4$, $Gr = 0.1 \times 10^4$, $\delta_i = 0$ $(i = 2, 3)$.

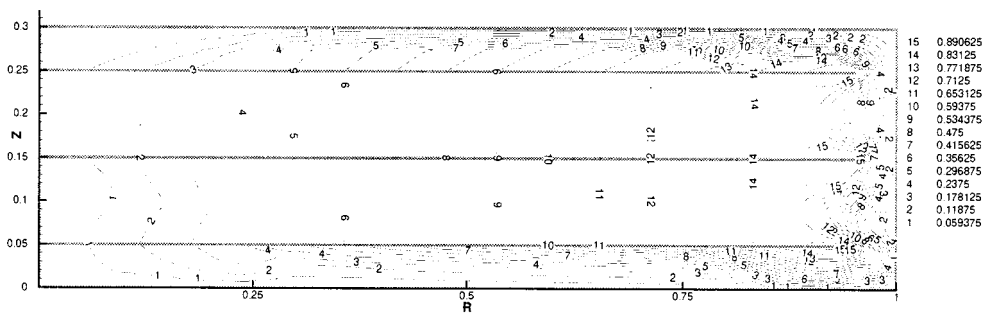

Figure 7. Swirling velocity for a three-disk system with $Re_\phi = 1 \times 10^4$, $Gr = 0.1 \times 10^4$, $\delta_i = 0$ $(i = 2, 3)$.

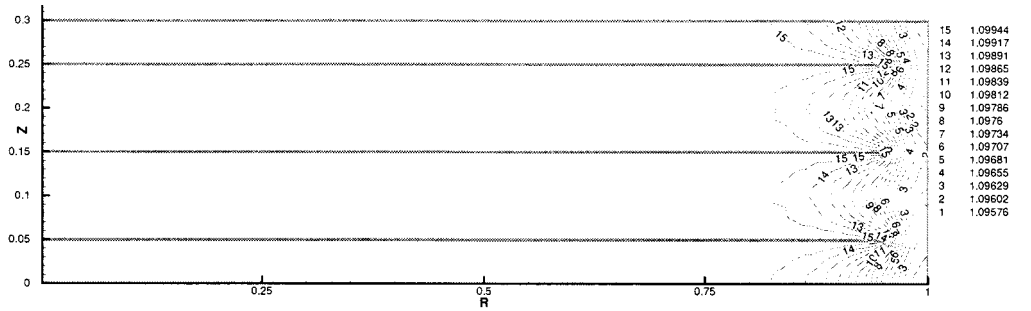

Figure 8. Isotherms for a three-disk system with $Re_\phi = 1 \times 10^4$, $Gr = 0.1 \times 10^4$, $\delta_i = 0$ $(i = 2, 3)$.

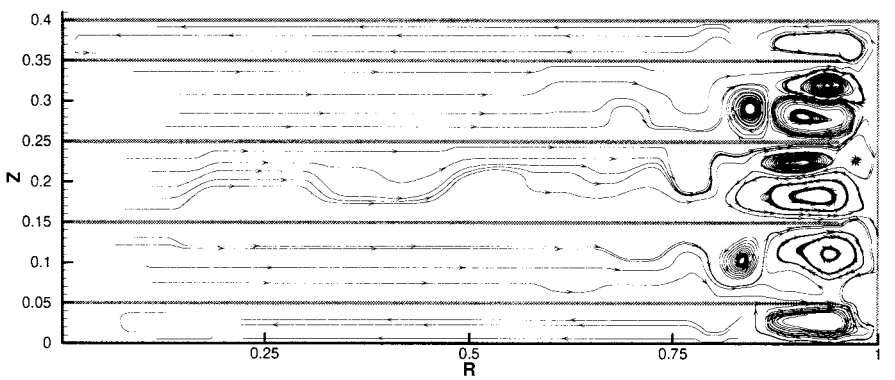

Figure 9. Streamlines for a four-disk system with $Gr = 0.1 \times 10^4$, $\delta_i = 0$ $(i = 2, 3, 4)$, $Re_\phi = 1 \times 10^4$.

In this work, an RNG k–ε model is used, inducing the buoyancy effect under the Boussinesq approximation. Other than the continuity equation (1), momentum equation (2) and energy equation (3), the RNG k–ε *turbulence model* are induced as follows:

$$\nabla\cdot(\rho\vec{u}\varepsilon) - \nabla\cdot\left(\frac{\mu_{\text{eff}}}{\sigma_{\varepsilon R}}\nabla\varepsilon\right) = \frac{\varepsilon}{k}\left(C_{\varepsilon_1 R}P - C_{\varepsilon_2 R}\rho\varepsilon\right) \tag{14}$$

$$\nabla\cdot(\rho\vec{u}k) - \nabla\cdot\left(\frac{\mu_{\text{eff}}}{\sigma_k}\nabla k\right) = P - \rho\varepsilon \tag{15}$$

where

$$C_{\varepsilon_1 R} = 1.42 - f_\eta; \quad f_\eta = \eta(1 - \eta/4.38)/(1 + \beta_R\eta^3); \quad C_{\varepsilon_2 R} = 1.68; \; \eta = (P/\rho C_{\mu R}\varepsilon)^{1/2};$$
$$C_{\mu R}\varepsilon = 0.085; \; \beta_R = 0.012.$$

An upwind difference scheme (UDS) combined with numerical advection correction (NAC) was used. NAC improves the accuracy by including a blending term

$$\phi_{ip} = \phi_n + \beta\phi_{\mathrm{NAC}}$$

where ϕ_{ip} is the variable at the centre of each surface segment in a three-dimensional element surrounding the finite volume; ϕ_n is the variable at the nodes of the element; β ranges from 0 (most robust) to 1 (second-order accurate but less robust).

The boundary conditions involved are: the enclosure is static with fixed temperature; for the multi-disks, the rotational speeds are given with fixed temperature too; for the axis, $u_i = 0$, $\partial T/\partial r = \partial\varepsilon/\partial r = \partial k/\partial r = 0$.

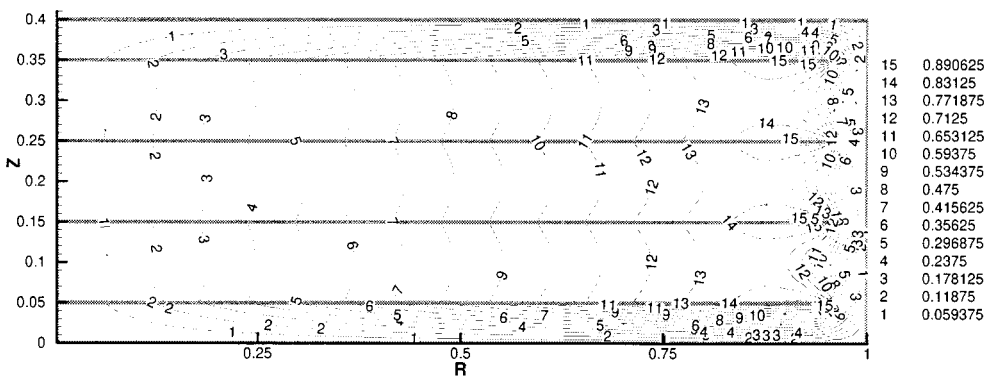

Figure 10. Swirling velocity for a four-disk system with $Gr = 0.1 \times 10^4$, $\delta_i = 0$ $(i = 2, 3, 4)$, $Re_\phi = 1 \times 10^4$.

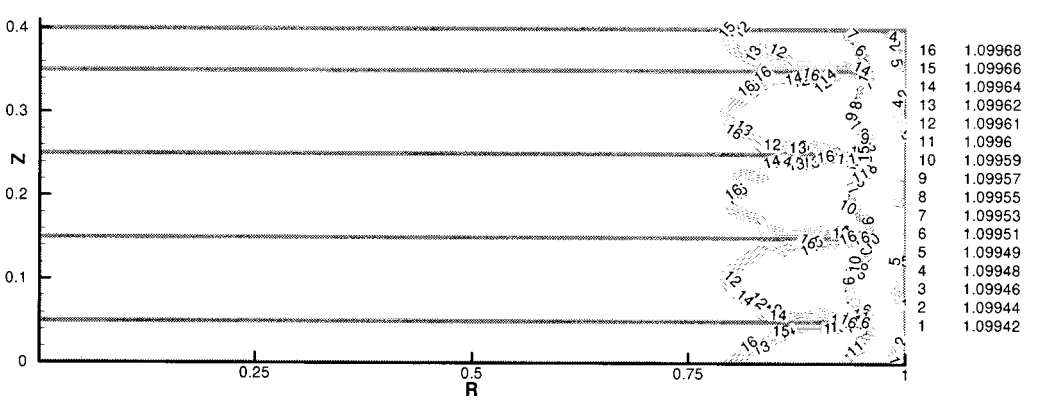

Figure 11. Isotherms for a four-disk system with $Gr = 0.1 \times 10^4$, $\delta_i = 0$ $(i = 2, 3, 4)$, $Re_\phi = 1 \times 10^4$.

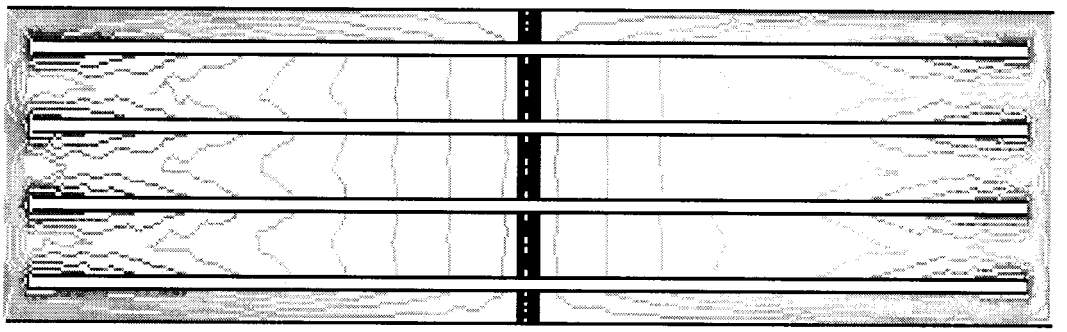

Figure 12. Swirling velocity for a four-disk system with $Gr = 0.1 \times 10^4$, $\delta_i = 0$ ($i = 2, 3, 4$), $Re_\phi = 1 \times 10^4$ (CFX).

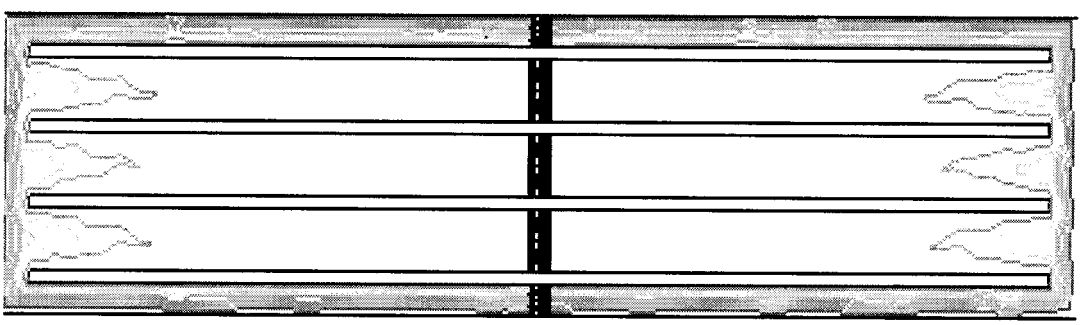

Figure 13. Isotherms for a four-disk system with $Gr = 0.1 \times 10^4$, $\delta_i = 0$ ($i = 2, 3, 4$), $Re_\phi = 1 \times 10^4$ (CFX).

CFX-5 uses a fully implicit discretization of the coupled equations at any given time step. The target residual for convergence is 10^{-6} with a maximum of 200 time steps. The time needed to run the program is about 2.5 min at each time step.

The multi-disk system with same flow conditions as in the FEM was chosen to simulate turbulent flow with $Gr = 0.1 \times 10^4$, $\delta_i = 0$ ($i = 2, 3, 4$), $Re_\phi = 1 \times 10^4$. Since the CFX-5 software uses the full three-dimensional model to compute, the results are also in three dimensions. The surface mesh of the four-disk system with a cylindrical enclosure was given in Figure 1 for CFX-5 and Figure 2 in the Z–R cross-sectional view by the current FEM respectively. However, for the comparison under the similar perspective, a slice plane in CFX-5 was selected to show the relative two-dimensional views qualitatively, which includes the contours of swirling velocity (Figure 12) and isotherms (Figure 13).

The swirling velocity predicted by the FEM code as shown in Figure 10 resembles the similar characteristic (computed by CFX-5) as presented in Figure 12. Higher velocity gradients

between the disk passages and enclosure are observed. The velocity contours within the inner disk spaces are almost periodic. Similarly, the isotherms computed by both the FEM (Figure 11) and CFX-5 (Figure 13) codes show the inward arc patterns near the outer disk end gaps.

6. CONCLUSION

The FEM using an RNG-based $k-\varepsilon$ model is developed to solve the multi-disk system within a cylindrical enclosure. The plots of flow structures and isotherms under different geometries and flow conditions are included. Similar results are obtained using a commercial code's prediction when the same flow conditions are imposed. It shows that the flow structure changes rapidly when Re_ϕ is increased—the flow has more tendency to flow radially outwards and the swirling velocity pattern tends to be more vertically distributed, especially for the high Re_ϕ value as in Figure 7. The isotherms, however, only have a small varying region near the axis, forming an outwards arc. With more realistic extensions, the work can be used to design an optimal disk structure with more stable flow and temperature profile, which is gradually becoming a problem when the rotational speed is high enough.

ACKNOWLEDGMENTS

The authors would like to thank Dr Z. Zhu of CSIRO, Australia and Professor C.Y. Soong of Chung Cheng Institute of Technology, Taiwan, for their valuable discussions and interest in the project.

REFERENCES

1. Brayan GH. The wave on a rotating liquid spheroid of finite ellipticity. *Philosophical Transactions A* 1889; **180**: 187.
2. Batchelor GK. Note on a class of solutions of the Navier–Stokes equations representing steady rotationally-symmetric flow. *Quarterly Journal on Mechanics and Applied Mathematics* 1951; **4**: 29–41.
3. Stewartson K. On the flow between two rotating coaxial disks. *Proceedings of the Cambridge Philosophical Society* 1953; **49**: 333–341.
4. Owen JM, Rogers RH. *Flow and Heat Transfer in Rotating-disc Systems: Rotor–Stator Systems*, vol. 1. Research Studies Press: UK, 1990.
5. Morse AP. Application of a low Reynolds number $\kappa-\varepsilon$ turbulence model to high-speed rotating cavity flows. *ASME Journal of Turbomachinery* 1991; **119**: 98–105.
6. Northrop A, Owen JM. Heat transfer measurements in rotating disc systems parts: the rotating cavity with a radial outflow of cooling air. *International Journal of Heat and Fluid Flow* 1987; **9**: 27–36.
7. Tzeng HM, Munce AC, Crawforth L. Quantitative visualization of surface flows on rotating disks. *Transactions of the ASME, Journal of Fluids Engineering* 1994; **116**: 494–498.
8. Yan WM, Soong CY. Simultaneously developing mixed convection in radically rotating rectangular ducts. *International Journal of Mass Transfer* 1995; **38**: 665–677.
9. Soong CY. Theoretical analysis for axisymmetric mixed convection between rotating coaxial disks. *International Journal of Heat and Mass Transfer* 1996; **39**: 1569–1582.
10. Soong CY, Chyuan CH. Navier–Stokes computations of non-isothermal flow and heat transfer between counter-rotating disks. In *Proceedings of the 6th International Symposium on Transport Phenomena and Dynamics of Rotating Machinery*, vol. 2, Han DC, Ro ST, Kim JH (eds). Pacific Center of Thermal-Fluids Engineering: Los Angeles, 1996; 39–46.
11. Morse AP. Assessment of laminar–turbulent transition in closed disk geometries. *ASME Journal of Turbomachinery* 1991; **113**: 131–138.

12. Morse AP, Ong CL. Computation of heat transfer in rotating cavities using a two-equation model of turbulence. *ASME Journal of Turbomachinery* 1992; **114**: 247–255.
13. Yakhot V, Orszag SA. Renormalization group. Analysis of turbulence: 1. Basic theory. *Journal of Scientific Computing* 1986; **1**(3).
14. Speziale CG, Thangam S. Analysis of an RNG based turbulence model for separated flows. *International Journal of Engineering Science* 1992; **30**(10): 1379–1388.
15. Thangam S, Speziale CG. Turbulent flow past a backward-facing step: a critical evaluation of two-equation models. *AIAA Journal* 1992; **30**(5): 1314–1320.
16. Zhu ZL. Numerical simulation of turbulent incompressible flows with a RNG based $k-\varepsilon$ model. In *First Asian CFD Conference*, Hong Kong, Paper 8c5. Asian CFD Society: Hong Kong, 1995; 1073–1078.
17. Zhu ZL. Artificial compressibility method with upwinding. In *Computational Techniques and Applications: CTAC93*, May RL, Easton AK (eds). World Scientific: Singapore, 1994; 502–510.
18. Liu ZY, Ng EYK. Simulation of flow in passage within the ventilated and non-ventilated rotating disks. *Computational Fluid Dynamics Journal* 1999; **7**(4): 485–494.
19. CFX International. *Using CFX–5*. AEA Technology Plc.: U.K, 2001; http://www.aeat.com/cfx.

